ANALYSIS OF SOLIDIFICATION PATH AND MICROSEGREGATION IN MULTICOMPONENT ALLOYS

William J. Boettinger, Ursula R. Kattner
Metallurgy Division
NIST
Gaithersburg, MD 20899, USA

and

Dilip K. Banerjee
UES, Inc.
Annapolis, MD 21401, USA

Abstract

The practical use of solidification modeling requires the treatment of multicomponent alloys. Significant progress has occurred in the development of thermodynamic databases for commercial alloys in recent years. Thermodynamic calculations using these databases with various microsegregation models are described. Effects of dendritic growth and solid diffusion on primary solidification and the continuation of the solidification path involving multiphase reactions are considered. Procedures to compute changes of enthalpy and density as functions of temperature during solidification are also reported.

Modeling of Casting, Welding and Advanced
Solidification Processes VIII
Edited by B.G. Thomas and C. Beckermann
The Minerals, Metals & Materials Society, 1998

Introduction

In this paper we consider the solidification path and resulting microsegregation occurring in castings of multicomponent alloys. Five topics will be discussed: the range of validity of the local equilibrium assumption, the description of phase diagram information using the CALPHAD method, predictions of a Scheil analysis including the formation of multivariant eutectics and peritectics, calculations of enthalpy and density changes during solidification, and deviations from the Scheil description caused by diffusion in the solid and dendrite tip kinetics.

Local Equilibrium Assumption

During all solidification processes, gradients of temperature and composition exist within the phases. However the growth kinetics can often be described using diffusion/convection transport modeling and using the equilibrium phase diagram to give the possible temperatures and compositions for the boundaries between the phases, e.g., at the solidification interface. The Gibbs-Thomson effect is included to determine shifts in equilibrium due to the curvature of the liquid-solid interface. This condition is called local equilibrium.

Local equilibrium is never strictly valid, but it is based on the notion that interfaces equilibrate much more quickly than bulk phases. Experiments to measure deviations from local equilibrium generally examine the velocity dependence of the partition coefficient, *k(V)*, for dilute alloys, defined as the ratio of C_S^* to C_L^*, the compositions at the interface of the solid and liquid. Analysis and experiments on doped silicon and metallic alloys (1) suggest that

$$k(V) = \frac{k_E + V/V_D}{1 + V/V_D} \qquad (1)$$

where k_E is the equilibrium partition coefficient and V_D is the diffusive speed that has been measured to lie between 6 and 38 m/s for different alloys. The velocity required to obtain a 1% variation in *k(V)* from k_E is $0.01 V_D k_E / (1-k_E)$ or between 0.06 and 0.38 m/s for $k_E = 0.5$. Such speeds are not usually found in castings. The deviation of the interface temperature from the liquidus is also negligible as long as *k(V)* is near k_E. Hence equilibrium phase diagrams are very useful for solidification modeling of castings. The effect of high speed solidification on microsegregation is described elsewhere (2).

Phase Diagram Information via the CALPHAD Method

The CALPHAD method (**cal**culation of **pha**se **d**iagrams) (3, 4) employs free energies of phases whose functional dependence on temperature and concentration approximate simple physical models for the atomic interactions in each phase. The concentration of the solid (or solids) in equilibrium with a given liquid concentration at a given temperature are obtained by equating the chemical potentials of each component in the coexisting phases according to standard thermodynamic principles.

Sets of free energy functions are available from the literature for many binary and some ternary systems. Numerical parameters for these functions are obtained by fitting the thermodynamic data (calorimetry, vapor pressure, emf, etc.) and the experimental phase diagram. For higher order systems, considerable success has been reported (5, 6) using a thermodynamic treatment of the ternary subsystems and employing a thermodynamic extrapolation method to treat the quaternary and all higher order systems.

Several groups have coupled thermodynamic calculation of phase diagrams to solidification models (see refs. in (7)). For the present work, it has been found convenient to describe the phase relationships with three subroutines of code: ***LEVER, SLOPE*** and ***HEAT***. These subroutines have been prepared using a modified version of the PMLFKT code developed by Lukas et al. (8). Output is available in either an atomic or mass (weight) basis. ***LEVER*** gives a list of all phases present at equilibrium (liquid L and solid phases α) , their compositions, $C_{L\,i}$ and $C_{\alpha\,i}$, and their mole or mass fractions, f_L and f_α , for a specified temperature T and overall composition, $C_{0\,i}$. This subroutine represents the standard "lever rule" relationship. It is used to determine when solid phases start or stop forming. ***SLOPE*** gives the liquidus temperature, $T_{L\alpha}$, the solid phase concentrations, $C_{\alpha\,i}$, and the liquidus slopes, $m_{\alpha\,i} = \partial T_{L\alpha} / \partial C_{Li}$, for a specified liquid composition and for each solid phase α on the list. ***HEAT*** gives the enthalpy per unit mass or per mole for each phase, H_α , on the list for a given temperature and phase composition. In symbolic form they are:

$$\begin{aligned} \textbf{\textit{LEVER}}: &\quad (T,\ C_{0i}) \Rightarrow (list,\ C_{Li},\ C_{\alpha i},\ f_\alpha) \\ \textbf{\textit{SLOPE}}: &\quad (C_{Li},\ list) \Rightarrow (T_L,\ C_{\alpha i},\ m_{\alpha i}) \\ \textbf{\textit{HEAT}}: &\quad (list,\ T,\ C_{\alpha i}) \Rightarrow (H_\alpha) \end{aligned} \qquad (2)$$

Table 1 shows two examples of the output of the subroutine ***SLOPE*** for the FCC phase for two commercial Al alloys. Here the data base developed by Saunders has been employed (9). Clearly the values for m_i and k_i are different for some of the solutes in the two alloys. The ability to determine the concentration dependence of these parameters is a great advantage of the thermodynamic approach. Other thermodynamic software can also be used to deliver phase diagram information to process models (10).

Table 1 - Example of output from ***SLOPE*** subroutine using Al database from Saunders (9). The units of concentration are wt% and of liquidus slope are °C/wt%. Al is treated as the solvent.

	T_L(°C)		Al	Si	Fe	Cu	Mn	Mg	Zn	Ti
A356	624	C_{Li}	---	6.0	0.2	0.2	0.1	0.35	0.1	0.2
		C_{Si}	---	0.69	.003	.023	.038	0.065	.047	0.93
		m_i	---	-6.86	-2.11	-3.19	-1.27	-2.85	-2.06	15.8
		k_i	---	0.11	.015	0.12	0.38	0.19	0.47	4.67
2219	642	C_{Li}	---	0.1	0.2	6.3	0.3			
		C_{Si}	---	.012	.005	0.21	0.64			
		m_i	---	-6.41	-3.35	-2.76	-1.84			
		k_i	---	0.12	.025	0.10	0.72			

Scheil Solidifications Paths in Multicomponent Alloys

Instead of modeling the diffusion in the liquid and solid phases in the mushy region of a casting, a simpler approach is commonly used as a good approximation for alloys whose solid phases are substitutional solid solutions. In any small volume of the mushy region whose temperature can be considered as uniform, it is reasonable to treat the liquid as uniformly mixed and the solid concentration as unaltered once frozen. In this approach, the Gibbs-Thomson effect and transport of solute in or out of the volume under consideration either by diffusion or convection are also

neglected. The beauty of this approach is its independence on the rate of cooling and on the details of the microgeometry of the liquid and solid regions within the volume of interest.

The Scheil path can be computed quite simply using the ***LEVER*** subroutine. At each specified temperature step during cooling, one computes the fraction of liquid, f_L, and the fractions of each solid phase, f_α , the concentration of the remaining liquid and the concentration of each solid phase formed during the step by the following procedure. Call ***LEVER***, using an overall concentration equal to the liquid concentration from the previous step and using the temperature of the present step. Update the remaining liquid concentration as equal to the liquid concentration output from ***LEVER***. Compute the increments of each phase formed Δf_α as $f_L f_\alpha{}'$ where f_L is the fraction liquid remaining from the previous step and $f_\alpha{}'$ is the phase fraction of each solid phase α on the list obtained from the call to ***LEVER***. Update the phase fractions amounts.

This procedure naturally treats the appearance of new phases at eutectic reactions, or the disappearance of phases at peritectic reactions. It determines the transition temperature to an accuracy determined by size of the temperature step used for the calculation during cooling. The precise transition temperature can be found by determining the temperature where the phase fraction of a new phase is exactly zero. Such a procedure is used in the computation of the Scheil path as performed in Thermo-Calc (11).

It is worth commenting on reactions with peritectic character. These include "reactions" such as $L+\alpha \rightarrow \beta$, $L+\alpha \rightarrow \beta + \gamma$ and $L+\alpha +\beta \rightarrow \gamma$, and higher order reactions, which may occur at a fixed temperature or over a range of temperatures depending on the number of components according to the phase rule. In all of the "reactions," one or more solid phases are consumed and replaced by another solid phase or phases. Whereas three mechanisms can form these new phases via peritectic "reaction"(2), all but one requires some diffusion in the solid, which to be consistent with the assumptions of the Scheil approach, must be ignored. Indeed most important for substitutional alloys is the formation of the new solid phase or phases directly from the melt. Thus when the solidification path encounters a "reaction" with peritectic character, the amount and concentration profile of the "consumed" phase becomes fixed and solidification of the remaining liquid proceeds with formation of the new phase or phases directly from the melt.

As an example, three Ni-Al-Ta alloys are chosen to give quite different solidification paths: (i) Ni-15at%Al-2at%Ta, (ii) Ni-20at%Al-1at%Ta and (iii) Ni-9at%Al-8at%Ta. The fraction solid vs. temperature relations for Equilibrium (Lever Law) and Scheil solidification were calculated using the database given by (12) and are given in Fig. 1. The liquid concentration paths are shown in Fig. 2 superimposed on the phase diagram. The primary phase for all alloys is the FCC-γ phase and is the only phase to form in each

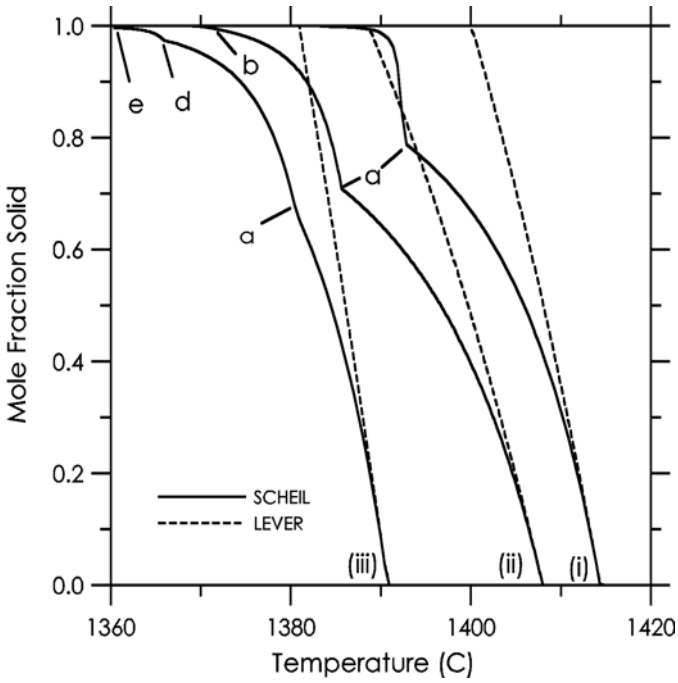

Figure 1 - Fraction solid vs. temperature for (i) Ni-15at%Al-2at%Ta, (ii) Ni-18at%Al-1at%Ta and (iii) Ni-9at%Al-8at%Ta with no solid diffusion (Scheil limit) & with complete solid diffusion (Lever limit).

alloy under equilibrium conditions. Under Scheil conditions, all three alloys encounter the $\gamma+\gamma'$ monovariant eutectic at points (a) in Figs. 1 and 2. Due to the temperature maximum in the monovariant eutectic line (shown by the bold dot), alloy (i) follows the monovariant eutectic line toward the binary Ni-Al side starting at a fraction solid of 0.79 and 1393°C. This line changes character to a monovariant peritectic line near the binary, but the fraction solid reaches 0.999 (taken as the end of solidification) before this point. The path for alloy (ii) does indeed reach this point and wanders off of the monovariant line (pt. b), following the surface of solidification of γ'. Thus γ' in this alloy would be formed both by "eutectic" and "peritectic" solidification, although it may be difficult to distinguish microstructurally. Finally a very small (0.01 mole fraction) of the β (B2-NiAl) phase is formed by the monovariant eutectic reaction, $L \rightarrow \gamma'+\beta$ near pt. c. For alloy (iii), the monovariant eutectic line, $\gamma+\gamma'$, is followed in the other direction, toward higher Ta content starting at a fraction solid of 0.66 and 1381°C. At a fraction solid of 0.98 and 1366°C, the path encounters the four phase reaction, $L+\gamma' \rightarrow \gamma+\pi$ (pt. d in Fig. 1 & 2). Under Scheil assumptions the fraction and concentration profile in the γ' phase becomes fixed and solidification continues along the monovariant $\gamma+\pi$ eutectic line. Finally at a fraction solid of 0.997, solidification is completed with the ternary eutectic reaction, $L \rightarrow \gamma+\pi+Ni_3Ta$ at 1360°C (point e in Figs 1 & 2). Fig. 3 shows the composition of the individual solid phases for alloy (iii) as a function of total fraction solid and represents the final microsegregation pattern in the solid.

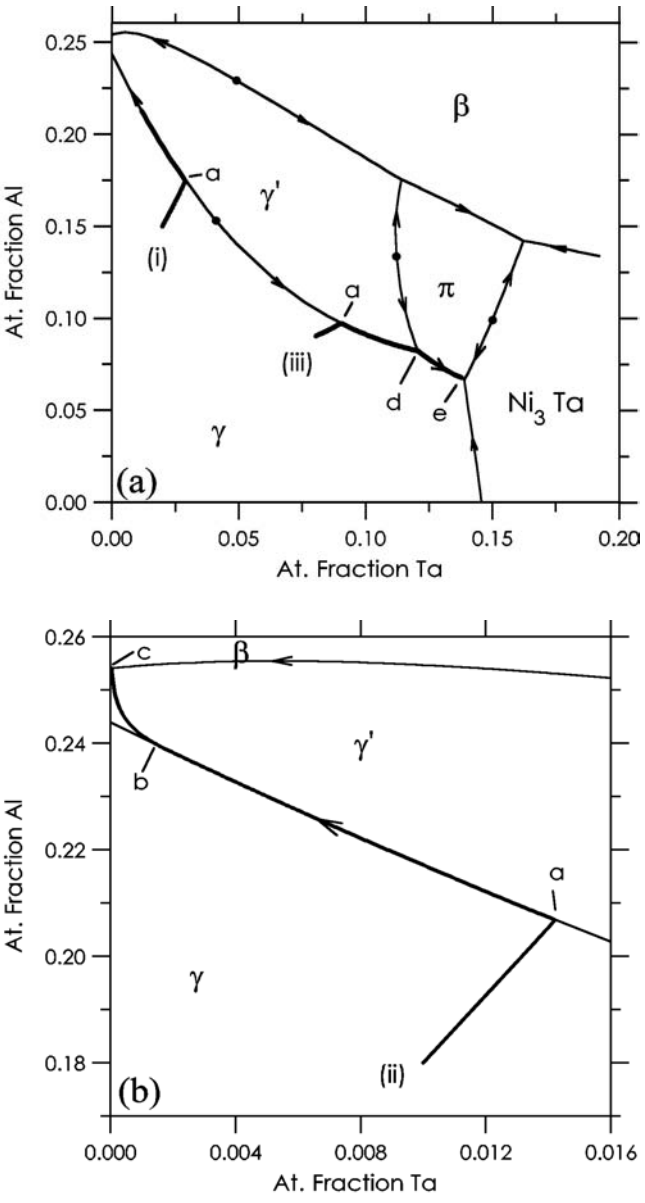

Figure 2 - (a) & (b) Solidification path (Al vs. Ta liquid concentration during cooling) in the Scheil limit superimposed on the Ni-rich corner of Ni-Al-Ta phase diagram for alloys (i) Ni-15at%Al-2at%Ta, (ii) Ni-18at%Al-1at%Ta and (iii) Ni-9at%Al-8at%Ta.

Finally a comment on metastable solidification paths is appropriate. Suppose that, in a complex solidification path involving many secondary phases, experimental information is obtained that a particular phase predicted by the Scheil analysis is absent in the microstructure. One approach to providing a solidification path is to assume that this phase has difficulty in nucleating. A new Scheil computation can be performed excluding this phase from the thermodynamic database. An obvious example is the exclusion of graphite from the solidification path in white cast irons.

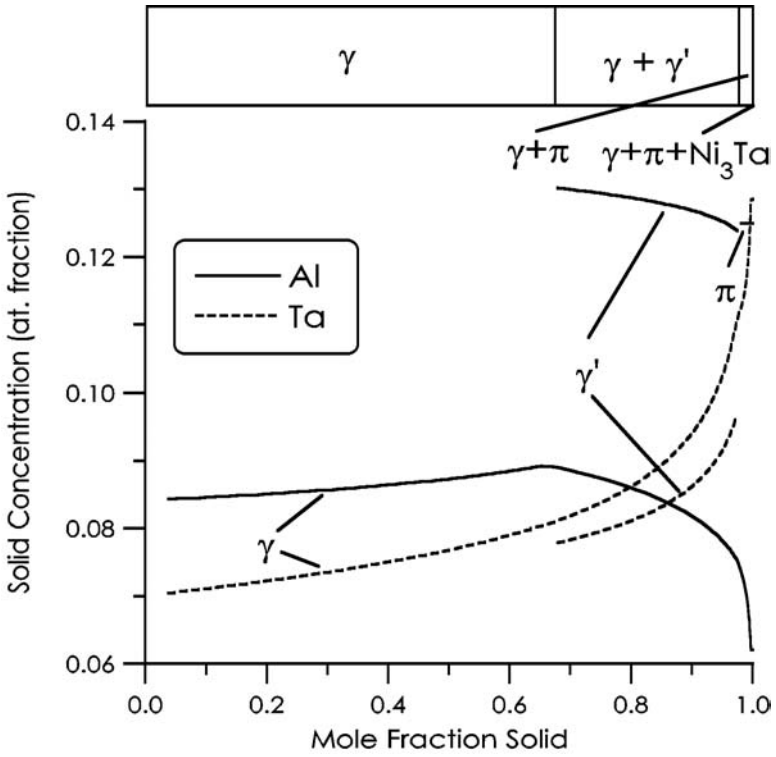

Figure 3 - Solid phase compositions vs. total fraction solid for alloy (iii) Ni-9at%Al-8at%Ta. The π-phase is Ni_6AlTa. The Ni_3Ta phase is not shown.

Enthalpy and Density Predictions

The enthalpy-temperature relation, *H(T)*, is very important in macroscopic modeling of heat transfer in castings. It is computed according to

$$H(T) = f_L \; H_L(C_{Li}, \; T) + \sum_{\alpha} f_\alpha \; H_\alpha(<C_{\alpha i}>, \; T) \qquad (3)$$

where H_L and H_α are the enthalpies per unit mass or mole of the liquid phase and solid phases. Due to the microsegregation in the solid phases, the enthalpy of the solid phases is computed at each temperature with a call to the subroutine, ***HEAT,*** based on their average concentrations, $<C_{\alpha i}>$ existing at that temperature. During computation of the Scheil solidification path described above, the change in average concentrations of each solid phase at each temperature step, $\Delta<C_{\alpha i}>$ are computed from $\Delta<C_{\alpha i}> = \Delta f_\alpha \, (C_{\alpha i} - <C_{\alpha i}>)/f_\alpha$, using the value of $<C_{\alpha i}>$ and f_α from the previous step and the value of $C_{\alpha i}$ from the current call to ***LEVER***. When a new phase appears, the initial value of $<C_{\alpha i}>$ is set to $C_{\alpha i}$ obtained from ***LEVER***. In principle the concentration profiles could be stored and a more exact computation of the solid phase enthalpies performed.

The enthalpy of each phase and the total enthalpy were computed for the Ni-9at%Al-8at%Ta alloy for Scheil solidification as shown in Fig. 4. The difference in enthalpy between the liquid and each solid phase is the heat of fusion for that phase. As is well known, the heat of fusion is larger for intermetallic phases than for the chemically disordered phases such as γ. The total enthalpy for a Lever calculation is also shown for comparison. The phase enthalpies in this case are omitted for clarity. Since heat flow codes that model castings require enthalpy/volume not enthalpy/mass or mole, either density versus temperature or molar volume versus temperature data are required.

Indeed, the density itself is of interest for the modeling of fluid flow in the mushy zone to predict macrosegregation and/or porosity. In principle, the molar volume of each phase can be treated in the same manner as its free energy by combining the values for the pure components and evaluating volume of mixing terms. Unfortunately no one has assembled such a data base for multicomponent alloys. Thus density data from other sources must be used.

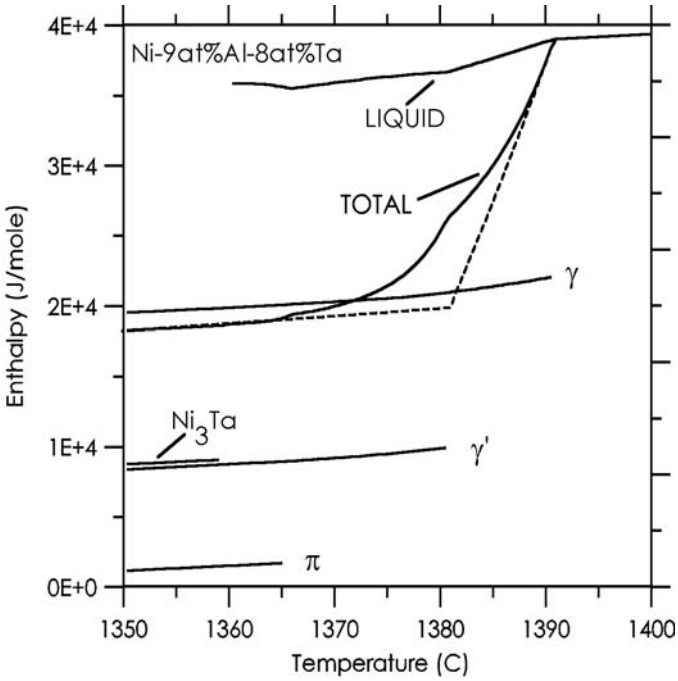

Figure 4 - Total enthalpy and phase enthalpies as a function of temperature during Scheil solidification for Ni-9at%Al-8at%Ta. The dashed curve is the total enthalpy for Equilibrium solidification.

Recently Sung et al. (13) have analyzed the densities, $\rho_L(C_{L\,i}, T)$ and $\rho_\gamma(C_{\gamma\,i}, T)$ of liquid and solid (γ-phase) superalloys, as functions of composition and temperature using a regression analysis. Using these results combined with an analysis of the solidification path, the liquid and γ-phase densities can be computed as a function of temperature only. The average concentrations of the solid phase can be used to compute the solid phase density as was done for the enthalpy. The overall density, allowing for the possibility of several solid phases and the formation of a volume fraction of porosity, f_p, is

$$\rho = (1 - f_P)\left\{\frac{1}{f_L^M/\rho_L + \sum_\alpha f_\alpha^M/\rho_\alpha}\right\} \qquad (4)$$

where f_L^M and f_α^M are mass fractions of the liquid phase and solid phases. For the modeling of microporosity, f_P must be determined as a function of temperature by other considerations. For example in the absence of dissolved gas, a simple model would calculate the porosity as that required to reduce the density change to a level where a negative pressure would not occur in the fluid.

In the absence of porosity, Fig. 5 shows the computed densities vs. temperature for a Ni-6wt%Al-8wt%Cr-6wt%Ta alloy. The solidification path has been computed with the Scheil assumption using the Dupin thermodynamic database (12) and a revised Ni-Al-Cr ternary (14). Solidification of γ is followed by γ+γ′ multivariant eutectic beginning at 1339°C with a switch at 1314°C to another multivariant eutectic, γ +β-NiAl, which completes solidification. Only a small fraction of β forms (0.007). As shown in Fig. 5, the liquid density decreases with cooling below the liquidus while γ and γ+γ′ form, but increases sharply as γ+β forms due to the large Al content of the β-NiAl phase and the fact that very little liquid remains. The decreasing liquid density with decreasing temperature can be a source of fluid flow instability and freckle formation during vertical directional solidification. Schneider et al. (15) have performed finite difference convection calculations of freckle formation using the ***SLOPE*** subroutine in a fully coupled manner. Also shown in Fig. 5 are the solid density and total density. Because separate density relations for γ′and β are not available, we have computed their densities using the expression for γ.

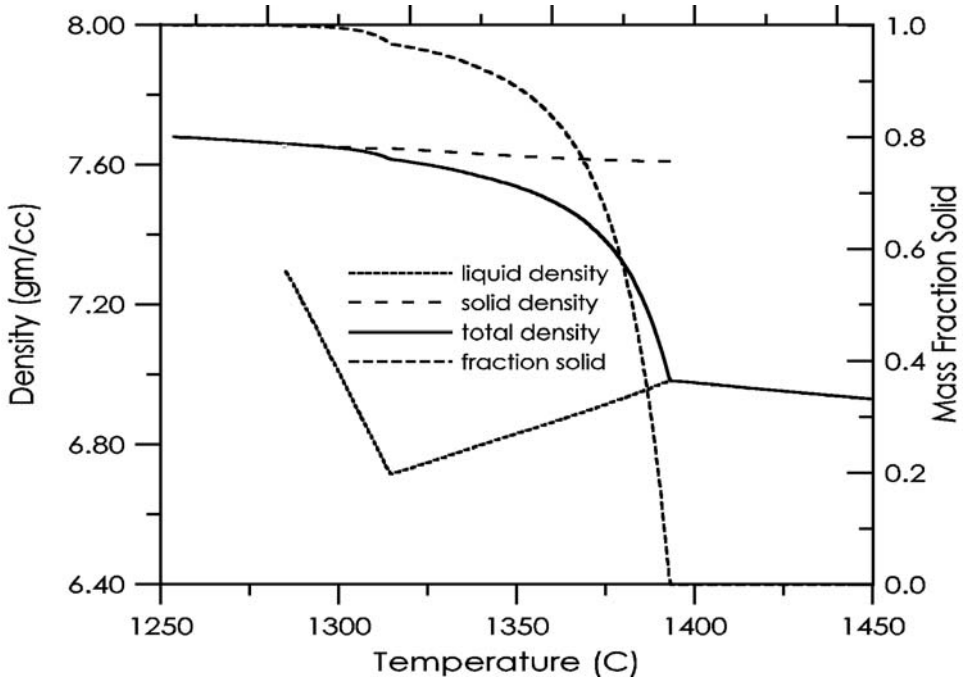

Figure 5 - Mass fraction solid, liquid density, solid density and overall density (if no porosity forms) as a function of temperature for a Ni-6wtAl-8wt%Cr-6wt%Ta alloy. The solidification path is predicted from a Scheil analysis. The densities are computed using relationships established by (13).

Effect of Solid Diffusion

Unlike calculations done with the Scheil approach, solid or back diffusion can not be treated without assumptions regarding the microgeometry of the liquid plus solid region and the time evolution of the fraction solid. During primary solidification, it is common to assume a plate, cylindrical or spherical geometry for dendrite (arms) to permit the treatment of diffusion in the solid in one dimension. In some models, the fraction of solid is assumed to be parabolic in time. Alternately, the evolution of fraction solid with time can be coupled to an enthalpy balance for inclusion into a macroscopic heat flow code (16).

For a well mixed liquid, a system of simultaneous equations is solved for a given time increment *dt* and enthalpy change *dH*. The solution gives the change in temperature *dT*, consistent with the solidification model, as well as the changes in liquid concentrations dC_L^i, solid phase fractions df_α average solid concentrations $d<C_\alpha^i>$ for each of the solutes and solid phases since the previous time step. Rather than solving the diffusion equations in the solid, an approximation that follows the approach of Wang and Beckermann (17) is quite useful, especially if coupling to a maco-model is required. For the case where a single solid phase α is forming, the following equations are solved for the incremental quantities.

$$C_p dT - L_\alpha df_\alpha = dH \tag{5}$$

$$f_L dC_{Li} + [<C_{\alpha i}> - C_{Li}] df_\alpha + f_\alpha d<C_{\alpha i}> = 0 \tag{6}$$

$$[<C_{\alpha i}> - C_{\alpha i}] df_\alpha + f_\alpha d<C_{\alpha i}> = \frac{12 D_{\alpha i} dt}{\lambda_2^2 f_\alpha} [C_{\alpha i} - <C_{\alpha i}>] \tag{7}$$

$$\sum_{1}^{n} m_{\alpha i} dC_{Li} = dT \qquad (8)$$

where λ_2 is the secondary arm spacing and $D_{\alpha i}$ are the solid diffusion coefficients. Off-diagonal diffusion coefficients have been neglected. Eqn. 5 guarantees that the enthalpy change is consistent with the change in fraction solid through the latent heat L_α and the change in temperature through the heat capacity C_p. Eqn. 6 and 7 guarantee solute conservation in the entire volume and the α phase, respectively. Eqn. 8 guarantees that the liquid concentrations remain on the α liquidus using the liquidus slopes, $m_{\alpha i}$.

The above treatment only deals with the primary solidification product. The treatment of solid diffusion during solidification involving multivariant eutectic or peritectic reactions requires additional assumptions about the solidification geometry that have only been attempted by a few authors (18-20). In the present calculations at each time step, the solution procedure checks the phase stability using the ***LEVER*** subroutine for the current temperature and liquid concentration and updates the list of solid phases forming. After primary solidification is completed, back diffusion is ignored.

Quantitative results for fixed cooling rates (not using Eqn. 5) are shown in Fig. 6 and 7 for the Ni-15at%Al-2at%Ta alloy. The fraction solid vs. temperature curves lie much closer to the Scheil limit than to the lever limit. The liquid concentration paths bend towards increased Ta levels as the cooling rate is decreased from the Scheil limit because $D_\gamma^{Ta} < D_\gamma^{Al}$, despite the fact that the lever path lies at lower Ta levels (see below). The cooloing rate dependence of the end points for solidification (here taken as f_s=0.998) is also shown. The final fraction of γ′ decreases from 0.13 to 0.10 as the cooling

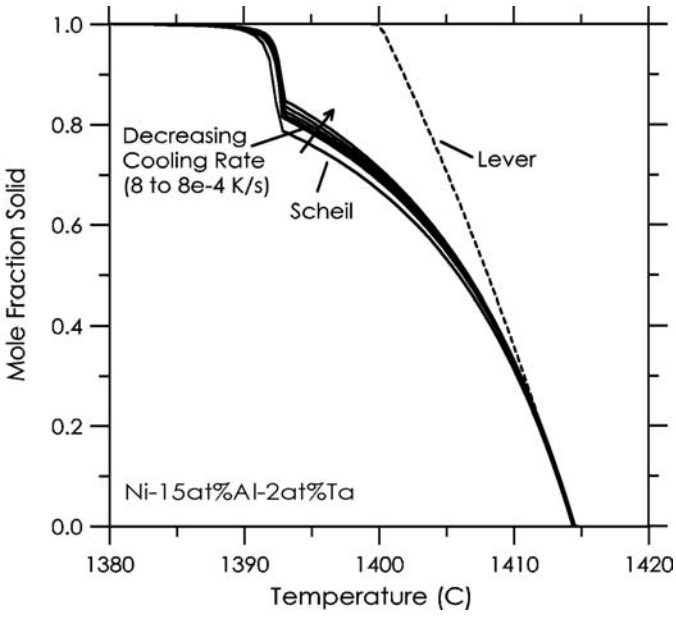

Figure 6 - Effect of solid diffusion on the liquid concentration path of Ni-15at%Al-2at%Ta for cooling rates ranging from 8 to 8x10^{-4} K/s.

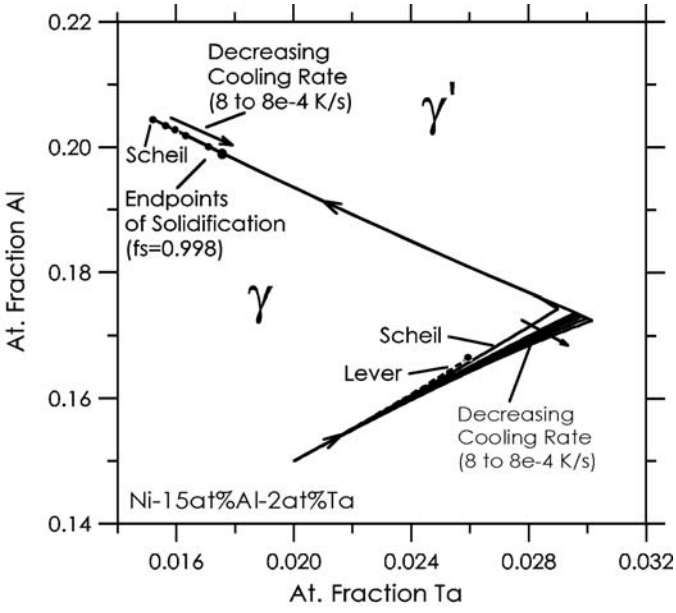

Figure 7 - Effect of solid diffusion on the fraction solid versus temperature curves for Ni-15at%Al-2at%Ta for cooling rates ranging from 8 to 8 x10^{-4} K/s in powers of ten.

rate decreases over the indicated range. The cooling rate was used to set λ_2 following a fit to data for Ni-base alloys given by (21). The values chosen for D_γ^i were the same as those used in (22).

It is interesting to explore some general features of solid diffusion during solidification of multicomponent alloys for unequal values of the solid diffusion coefficients. To isolate the effects of such differences, Fig. 8 shows schematic solidification paths for the primary phase for a ternary system where the liquidus slopes and partition coefficients are constant and equal respectively for the two solutes. Thus, the Scheil and lever solidification paths are straight lines with slopes of unity on a Cartesian plot of the two solute concentrations. The beginning point of both paths is the initial liquid concentration. The end points of the two paths (taken as $f_S = 0.99$ say) path are different. Also indicated are several paths for decreasing cooling rates if $D_S^1 < D_S^2$. For the purpose of this discussion, the paths are drawn for the primary phase only and thus some paths extend beyond the eutectic valley along the extrapolated primary liquidus surface. The paths will bend toward increased levels of component #1. The locus of the end points for decreasing cooling rates swings away from the Scheil path but must eventually return to the end pont for the lever path in the limit of very slow cooling. In a case of unequal *m's* and/or *k*'s, if the end point of the lever path is, for example, above the Scheil path, the locus of end points would swing below the Scheil path before crossing over the Scheil path as the cooling rate is decreased. This occurs in Fig. 7.

These trends can produce results not possible in binary systems regarding the effect of solid diffusion on the fraction of second phases. Fig. 8 also shows how the paths might intersect eutectic valleys that have different orientations with respect to the solidification path. In Fig. 8a, decreasing the cooling rate would increase the value of f_s where the path hits the eutectic valley. This will decrease the fraction of eutectic in the final microstructure. In Fig. 8b, the path intersects the eutectic valley at smaller values of f_s as the cooling rate is initially decreased from the Scheil limit. The fraction of eutectic would first increase and then decrease as the cooling rate is decreased.

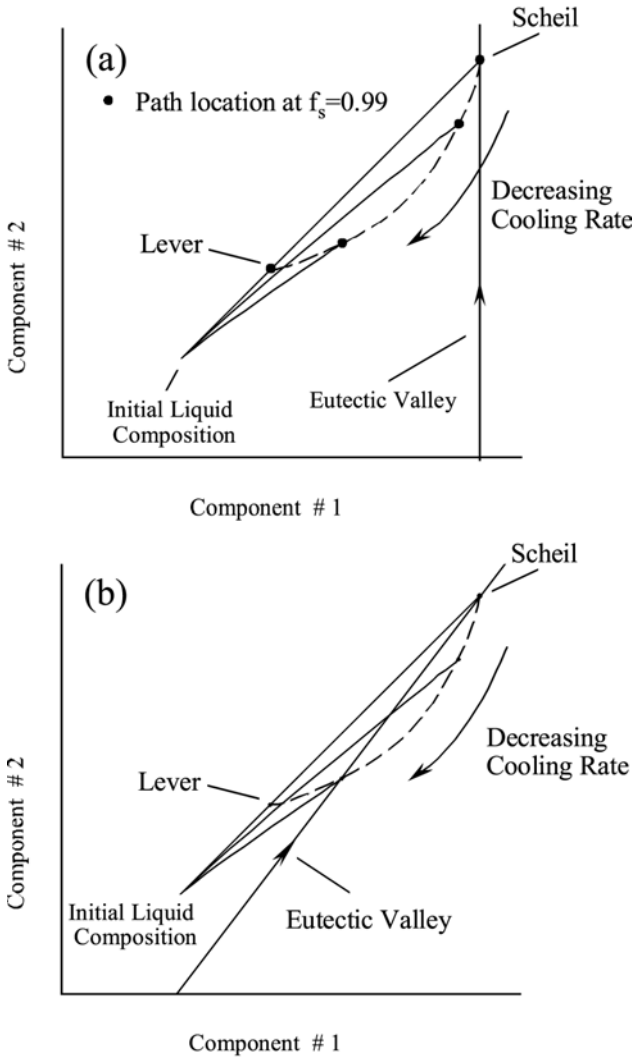

Figure 8 - Schematic representation of the change in solidification path shape for the primary phase depending on cooling rate when the solid diffusion coefficients of the solutes in the solid are unequal, $D_S^1 < D_S^2$. Also shown are the intersection of the solidification paths with eutectic valleys with two different orientations. In a) the fraction of eutectic would decrease and in b) the fraction of eutectic would increase as the cooling rate is decreased from the Scheil limit.

Effect of Dendrite Tip Kinetics

Tip Conditions - In the above discussion, transport of solute in the liquid phase was assumed to be sufficiently rapid that the liquid could be considered uniform in concentration during cooling. Including liquid diffusion through a consideration of the kinetics of dendritic growth lead to a lowering of the temperature where solidification first begins.

The equations that govern the dendritic growth of the primary phase of an n-component alloy with (n-1) concentrations, $C_{0\,i}$, at velocity, V, and temperature gradient, G, have been derived by several authors (23, 24). The values of the (n-1) concentrations at the dendrite tip, $C_{L\,i}^{*}$, differ from the nominal alloy concentrations due to the requirements for liquid diffusion. Solution of the governing equations, which involve the Ivantsov diffusion solution in the liquid and the marginal stability analysis of the tip radius, is accomplished using the subroutine ***SLOPE*** to determine T_L, k_i and m_i at $C_{L\,i}^{*}$ for the solid phase growing dendritically. Examples of the undercooling-velocity relationship obtained by this procedure are shown in ref. (25). The results for zero temperature gradient would be customarily used for the simulation of equiaxed castings and for the cellular automaton simulations of Gandin and Rappaz (26). The tip speed vs. temperature relation can be fit with a polynomial function to reduce computation times.

Subsequent Solidification Path - Coupling of the dendrite tip analysis to the description of the solidification path at temperatures below the dendrite tip temperature have been performed for binary alloys by several authors (17, 27, 28). Frequently, however, a simpler approach is used to couple the dendrite tip analysis to the remainder of the solidification path.

The "truncated Scheil" method, proposed by Flood and Hunt (29), develops the fraction solid vs. temperature curve by assuming that, during cooling, the fraction of solid jumps from zero to the value given by the standard Scheil analysis at the temperature at which the dendrite tip is operating. This approach is extremely attractive for its simplicity and has been employed by Gandin and Rappaz (26). With this approach the effect of dendrite tip kinetics on the variations in fraction of second phases can not be determined because the total amount of solute is not conserved.

This deficiency can be corrected by an alternate procedure (25) that makes a call to ***LEVER*** at the temperature of the dendrite tip for an overall concentration equal to the initial alloy concentration. This gives a fraction of solid that should form in the tip region and also determines the concentrations of the remaining liquid just behind the tip region. The liquid concentration and fraction solid so obtained are then used as the initial values for a subsequent solidification path calculation using the methods described above. This procedure conserves solute if the liquid diffusion coefficients are equal and the effect of the Gibbs-Thomson effect on the tip concentration can be neglected. In other words, the liquid concentration obtained from the call to ***LEVER*** will equal the liquid concentration at the tip, $C_{L\,i}^{*}$. For slow dendritic growth rates however, the simpler "truncated Scheil" approach is an excellent approximation for many cases (25). A full coupling of macroscopic heat flow and the dendrite tip undercooling and speed for columnar growth has been performed by M'Hamdi et al. (30).

Conclusion

Phase diagram information for multicomponent alloys, which is computed through a thermodynamic approach, has been coupled to various solidification models to predict the solidification path and associated enthalpy and density changes.

References

1. P. M. Smith and M. J. Aziz, Acta Mater. **42** (1994) 3515.
2. H. Biloni and W. J. Boettinger, "Solidification", in Physical Metallurgy, 4th edition, edited by P. Haasen and R. W. Cahn, 1996, North Holland, Amsterdam, p. 669-842.
3. J. Agren, Current Opinion in Solid State & Materials Science **1** (1996) 355.
4. U. R. Kattner, J. of Metals, **49(12)** (1997) 14.
5. N. Saunders, Superalloys 1996 eds. R.D.Kissinger et al (TMS, Warrendale, PA, 1996), p.101.
6. N. Saunders, in Light Metals 1997, ed.R. Huglen (TMS, Warrendale, PA, 1997) p. 911.
7. T. Kraft and Y.A. Chang, J. of Metals, **49(12)** (1997) 20.
8. H. L. Lukas, J. Weiss, E.-Th. Henig, CALPHAD **6** (1982) 229-251.
9. N. Saunders, Materials Science Forum **217-222** (1996) 667.
10. B. Sundman, H. Sippola and G. Eriksson, CALPHAD XXIII, Madison, WI, 1994.
11. Q. Chen and B. Sundman, as implemented in version L of Thermo-Calc, Roy. Inst. of Tech., 1995, Stockholm, Sweden.
12. N. Dupin, Ph.D. Thesis, Lab. Thermo.et de Phys.-Chimie Métall. de Grenoble, France, (1995).
13. P. K. Sung, D. R. Poirier and E. McBride, Mat. Sci. & Eng. **A231** (1997) 189-197. Also P. K. Sung and D. R. Poirier, Mat. Sci. & Eng. in press.
14. W. Huang and Y. A. Chang, unpublished research, U. Wisconsin-Madison , 1997.
15. M.C. Schneider, J.P. Gu, C. Beckermann, W. J. Boettinger and U.R. Kattner, Met. Mat. Trans. A, **28A** (1997) 1517-1531.
16. D. K. Banerjee and M. T. Samonds, U. R. Kattner and W. J. Boettinger, in Solidification Processing, 1997, edited by J. Beach and H. Jones, Department of Engineering Materials, University of Sheffield, UK 1997, p.354.
17. C. Y. Wang and C. Beckermann, Mat. Sci. & Eng. **A171** (1993) 199.
18. S.-W. Chen and Y.A. Chang, Met. Trans. **23A** (1992) 1038.
19. C. Beckermann and M. Schneider, ISIJ International **35**(1995) 665.
20. K. Ohsasa, S. Nakuae, M Kudoh and T. Narita, ISIJ International **35** (1995) 629.
21. G. K. Bouse and J. R. Mihalsin, in Superalloys, Supercomposites and Superceramics, ed. by J. K. Tien and T. Caulfield, Academic Press, 1989, p. 99.
22. W. J. Boettinger, U. R. Kattner, S.R. Coriell, Y. A. Chang and B. A. Mueller, in Modeling of Casting, Welding and Advanced Solidification Processes, VII, eds. M. Cross & J. Campbell, TMS, Warrendale, PA, 1995, p. 649.
23. M. Bobadilla, J. Lacaze and G. Lesoult, J. Crystal Growth **89** (1989) 531-544.
24. M. Rappaz, S. A. David, J. M. Vitek and L. A. Boatner, Metall. Trans. A **21A** (1990) 1767-1782.
25. U. R. Kattner, W. J. Boettinger and S. R. Coriell, Z. Metallkunde, **87** (1996) 522-528.
26. Ch.-A. Gandin and M. Rappaz, Acta Metall. Mater. **42** (1994) 2233-2246.
27. M. Rappaz and Thévoz, Ph.: Acta Metall. **35** (1987) 1487-1497.
28. B. Giovanola and W. Kurz, Metall. Trans. A **21A** (1990), 260-263.
29. S.C. Flood and J. D. Hunt, J. Crystal Growth **82** (1987) 543-551.
30. M. M'Hamdi, H. Combeau, M. Bobadilla and G. Lesoult, in Solidification Processing, 1997, edited b